RESEARCH ARTICLE | DECEMBER 04 2023

Oblique water entry of a curved foil with varying speed

Shi Yan Sun (孙士艳) ; Fanrong Zeng (曾繁荣); Yifeng Yang (杨毅锋) ; Wenli Wang (王文丽)

Physics of Fluids 35, 122101 (2023)
https://doi.org/10.1063/5.0179113

Physics of Fluids ARTICLE pubs.aip.org/aip/pof

Oblique water entry of a curved foil with varying speed

Cite as: Phys. Fluids **35**, 122101 (2023); doi: 10.1063/5.0179113
Submitted: 29 September 2023 · Accepted: 14 November 2023 ·
Published Online: 4 December 2023

Shi Yan Sun (孙士艳),[1] Fanrong Zeng (曾繁荣),[1] Yifeng Yang (杨毅锋),[2,a)] and Wenli Wang (王文丽)[1]

AFFILIATIONS

[1]School of Naval Architecture & Ocean Engineering, Jiangsu University of Science and Technology, Zhenjiang 212003, China
[2]Department of Mechanical Engineering, University College London, Torrington Place, London WC1E 7JE, United Kingdom

[a)]Author to whom correspondence should be addressed: yifeng.yang.19@ucl.ac.uk

ABSTRACT

The hydrodynamic problem of a curved foil entering into water obliquely with varying speed is investigated through the boundary element method in time domain, and fully nonlinear boundary conditions on the deforming free surface are adopted. The process of foil entry begins with a single point at the lower edge; posing numerical challenges due to the extremely small wetted area, we utilize the stretched co-ordinate system method to address this. An auxiliary method is adopted to solve for pressure distribution. The whole process of the attached flow forming along the curved body and then detaching from the top edge is considered. We engage in extensive discussions on the effects of curvature, gravity, and acceleration, exploring their physical significance and potential applications, particularly within the context of surface-piercing propellers.

NOMENCLATURE

a	The acceleration of foil
c	Chord length
C_d	Drag coefficient
C_f	Force coefficient of a flat foil
C_p	Pressure coefficient
C_l	Lift coefficient
F_n	Froude number
$\boldsymbol{n}$	Normal vector
$O-x_0y_0$	Physical system
$O-\alpha\beta$	Stretched system
s	Both the distance of vertical entry of foil and the stretched ratio
S_b	Body surface
S_c	Far-field control boundary
S_f	Free surface
$\boldsymbol{U}$	Velocity vector of foil
u	The magnitude of horizontal velocity of foil
v	The magnitude of vertical velocity of foil
v_0	The initial vertical velocity of foil
α_0	The angle between velocity vector and horizontal axis
α_A	Attack angle
γ	deadrise angle
ε	The ratio of vertical entry velocity to horizontal velocity
ϕ	Velocity potential in physical system $O-xy$
φ	Velocity potential in stretched system $O-\alpha\beta$

I. INTRODUCTION

Surface-piercing propellers are specifically engineered to operate partially above the water surface, offering significant advantages in terms of efficiency, performance, and safety. The process of a surface-piercing propeller entering the water involves intricate changes in the deformation of the free surface and the rapid alteration of the blade's wetted area. In our current study, we delve into the investigation of a foil slice's entry, utilizing the well-established lifting line theory.[1]

In the past, much of the research in this field relied heavily on linearized free surface conditions as the basis for their investigations. When a foil enters the water, it leads to the departure of fluid from both edges of the foil, creating a cavity behind the plate. Researchers like Yim[2,3] applied linearized boundary conditions along with a conformal mapping technique to derive analytical solutions for the behavior of a ventilated flat plate as it entered an undisturbed free surface. Similarly, Wang[4,5] employed conformal mapping methods based on linearized boundary conditions to obtain analytical solutions for the behavior of both plates and circular arc foils with small deformation as they entered the water. However, it is important to note that the work

of Yim[2,3] and Wang[4,5] was primarily restricted to situations where the foil had a small attack angle. Another approach that relied on linearized boundary conditions was the negative mirror image method. In this approach, the velocity potential was assumed to be zero on the undisturbed flat free surface. Notable work in this field includes the research conducted by Furuya[6] and Young and Kinnas.[7] Furuya[6] used linearized boundary conditions to transform the governing equation for potential into one for pressure and then utilized a singularity distribution method for the solving of numerical problem. On the other hand, Young and Kinnas[7] employed a low-order boundary element method (BEM) to examine a system with a separated flow region and cavity effects. Similar investigations were carried out by Yari and Ghassemi.[8] These various methods and approaches have been instrumental in understanding the behavior of foils and plates as they enter into water, particularly in cases involving small attack angles.

In addressing the issue of nonlinear free surface boundary conditions, various approaches have been explored in past work. Chekin[9] investigated the self-similar flow of an inclined semi-infinite plate by employing the integral equation method within the complex plane. In this work, the profile of the free surface remains unknown and is an integral part of the solution. Savineau,[10] on the other hand, utilized the boundary element method (BEM) to analyze a finite curved plate with arbitrary shape. The shape of the cavity formed between the plate edge and the undisturbed free surface was updated through an iterative process, accounting to the nonlinear free surface boundary condition. Faltinsen and Senemov[11] employed the integral hodograph method to examine the self-similar flow of a semi-infinite plate without considering the influence of gravity. Their solution was attained through iterative techniques. In a different vein, Vinayan and Kinnas[12] integrated the boundary element method with fully nonlinear boundary conditions to model the water entry of a plate. A small plate, mirroring the shape of the cavity in the unbounded fluid domain,[13] was fixed to the lower edge of the primary plate. This auxiliary plate aimed to provide an improved initial condition and circumvent numerical challenges associated with the free surface at the edge of the main plate. The working assumption was that the influence of the small plate would diminish at later stages of the process. Sun and Wu[14] also explored the water entry phenomenon of an inclined plate under fully nonlinear boundary conditions. To mitigate numerical issues arising from singularities as the leading edge contacted the water, they adopted a stretched co-ordinate system. Furthermore, simulations of plate water entry related to surface-piercing propellers (SPP) have been conducted using more general computational fluid dynamics (CFD) techniques. These simulations predominantly rely on viscous flow theory, grounded in the Navier–Stokes equations. Noteworthy contributions include the work of Ghadimi and Javanmardi,[15] where a falling foil led to flow detachment from the leading edge, resulting in various types of trapped bubbles. Javanmardi and Ghadimi[16] explored a similar scenario but incorporated the elastic effects of the leading edge. Finally, Mesa *et al.*[17] addressed the problem of water entry for an inclined elastic plate. When the deadrise angle between the plate and the free surface approaches zero, the problem transforms into the scenario of a horizontal plate impacting the water surface. This specific case has been studied in prior works by researchers such as Iafrati and Korobkin,[18,19] Krechetnikov,[20] and Sun and Wu.[21] Most of the entry time, the cavity formed behind the plate ventilates to air, during this stage, the pressure inside the open cavity is the atmospheric pressure, but it would eventually be closed before the start of the next cycle; then, the variation of air pressure inside the closed bubble should be considered, and there was much work on bubble dynamics such as those by Cui *et al.*[22] and Wang *et al.*[23,24]

In the preceding research, within the scope of inviscid potential flow theory, work on the water entry of a curved plate is mainly based on linear assumption, and the nonlinear effect is important but rarely considered. The current study aims to address the water entry problem involving a curved foil at varying speeds while accounting for gravity effects. The approach taken involves the use of fully nonlinear boundary conditions for the deforming free surface shape, with the utilization of the boundary element method—an approach that has proven successful in related research by the authors.[14]

II. NUMERICAL MODEL AND MATHEMATICAL PROCEDURE

A. The mathematical model in physical system

In the lifting line theory, the two-dimensional lifting force of a foil of SPP depends on foil geometry, deadrise angle, and velocity and angle of entry. Thus, we consider the problem of a foil with an arc camber profile and a chord length c impacting a horizontal free surface, see Fig. 1. A Cartesian co-ordinate system $O-x_0y_0$ is defined, in which x_0 is along the undisturbed the free surface, y_0 points vertically upward, and the origin is fixed at the point where the tip of the plate touches the free surface initially. A local system $O-x_By_B$ is established with x_B and y_B that are, respectively, along and perpendicular to the foil chord, and the origin is fixed at the leading edge of foil. The foil has an inclined angle γ with the x_0 axis, which is also called deadrise angle in water entry problems. It enters into water with a velocity $\boldsymbol{U}=u\boldsymbol{i}-v\boldsymbol{j}$, where u and v are the velocity components along the x_0 and y_0 directions, respectively, and negative sign before v means that it is positive when the plate moving downward. $\alpha_0=\mathrm{atan}(v/u)=\mathrm{atan}(1/\varepsilon)$ is the angle between $\boldsymbol{U}$ and x_0 axis, and ε is the ratio of vertical entry velocity to horizontal velocity. In the paper, we use the water density ρ, the chord length c, and the initial vertical velocity v_0 for nondimensionalization. In the following paper, the signs are all nondimensionalized.

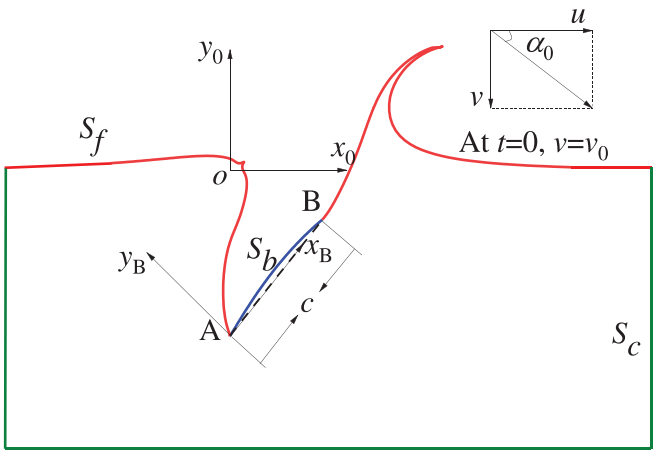

FIG. 1. Water entry of a foil.

The fluid is assumed to be ideal and incompressible, and the flow is irrotational. The velocity potential theory based on the Laplace equation can then be used. The governing equation for the potential ϕ in the fluid domain bounded by the free surface S_f, body surface S_b, and control boundary S_c can be written as follows:

$$\nabla^2\phi = 0. \tag{1}$$

On the plate surface S_b, the impermeable boundary condition takes the form of

$$\phi_n = un_{x_0} - vn_{y_0}, \tag{2}$$

where $\boldsymbol{n} = (n_{x_0}, n_{y_0}) = \left[\frac{\frac{\partial x_0}{\partial n}}{\sqrt{\left(\frac{\partial x_0}{\partial n}\right)^2+\left(\frac{\partial y_0}{\partial n}\right)^2}}, \frac{\frac{\partial y_0}{\partial n}}{\sqrt{\left(\frac{\partial x_0}{\partial n}\right)^2+\left(\frac{\partial y_0}{\partial n}\right)^2}}\right]$ is the normal of the body surface, pointing out of the fluid domain. On the free surface S_f, the Lagrangian form of the kinematic and dynamic conditions can be, respectively, written as follows:

$$\frac{dx_0}{dt} = \phi_{x_0}, \quad \frac{dy_0}{dt} = \phi_{y_0}, \tag{3}$$

$$\frac{d\phi}{dt} = \frac{1}{2}\left(\phi_{x_0}^2 + \phi_{y_0}^2\right) - \frac{y_0}{F_n^2}, \tag{4}$$

in which $F_n = v_0/\sqrt{gc}$. The temporal derivative d/dt is taken by following a fluid particle. In the Eulerian form, the kinematic and dynamic conditions can be written as follows:

$$\frac{\partial\eta}{\partial t} = \phi_{y_0} - \frac{\partial\eta}{\partial x_0}\phi_{x_0}, \tag{5}$$

$$\frac{\partial\phi}{\partial t} = -\frac{1}{2}\left(\phi_{x_0}^2 + \phi_{y_0}^2\right) - \frac{y_0}{F_n^2}, \tag{6}$$

where the temporal derivative is taken when x_0 and y_0 are fixed, and η is the elevation measured in z direction. As illustrated in Fig. 1, the flow detaches from leading edge A once it touches the water, and will also detach from trailing edge B when the free surface on the right surpasses the foil. These two points are simultaneously on the free surface and body, and the continuity condition should be imposed here

$$\eta_A = w_A,\ \eta_B = w_B, \tag{7}$$

in which w_A indicates the position of point A of the plate, while w_B indicates that of B, and $\eta_A = w_A$ means the location of the point of the free surface adjacent to point A is the same as the location of point A of the plate, so does the point B. The variation of ϕ should not only consider the variation of time, but also need consider the variation of position of edge A and B, which own velocities u and $-v$ with the motion of the whole rigid foil; then, the time derivative defined in this way can be written as follows:

$$\frac{\delta\phi}{\delta t} = -\frac{1}{2}\left(\phi_{x_0}^2 + \phi_{y_0}^2\right) - \frac{y_0}{F_n^2} + u\phi_{x_0} - v\phi_{y_0}. \tag{8}$$

$\frac{\delta\phi}{\delta t}$ means the derivative of ϕ with respect to t at the given position of edge A or B. Away from the plate, the fluid is assumed to be undisturbed by the plate motion. Then, the boundary condition at the boundary S_c takes the form of

$$\nabla\phi = 0. \tag{9}$$

To start the simulation, an initial condition has to be prescribed. Physically, as only a very small region of the fluid domain is disturbed, this is not expected to have lasting effect on the flow at the later stage. However, numerically a proper treatment of the initial condition is important for the simulation.[14] On the right-hand side, the free surface is assumed to be undisturbed. On the left, the local free surface near the tip of the plate is assumed to be perpendicular to the plate and then joins the undisturbed main free surface, and $\phi = 0$ is assumed on the free surface.

B. Stretched system

A particular feature of this kind of problem is that at the initial stage, there is only a small part of the body in contact with water, or the wetted surface is small. This part will increase as the plate moves into the water. This means that initially the disturbed region of the fluid is small, while within this region, the flow varies rapidly. To capture this variation, the size of a typical element used in a numerical method must be much smaller than that of the wetted surface. Later on the disturbed region will increase. To continue to use small elements would mean that a large number of them would be needed. Therefore, the element size should increase as the plate moves into water. To achieve this more effectively, we may use the stretched coordinate system method.[25] Let s be the vertical distance of the plate traveled into the water. We define

$$\alpha = \frac{x_0}{s}, \quad \beta = \frac{y_0}{s}, \quad \varphi = \frac{\phi}{s}. \tag{10}$$

This means that both the co-ordinates and the potential have been amplified by s. In such a way, the size of the disturbed domain remains more or less the same at the earlier stage when s is small and at the later stage when s is large. The element size and the element number can also remain more or less the same. When s is comparable to the dimension of the foil, for example, half the chord length $0.5c$, the computation may be conducted directly in the $O - x_0y_0$ system. Then, Eq. (1) will retain its form for φ, while Eqs. (2)–(4) and (8) become

$$\varphi_n = un_\alpha - vn_\beta \quad \text{on } S_b, \tag{11}$$

$$\frac{ds\alpha}{dt} = \varphi_\alpha, \frac{ds\beta}{dt} = \varphi_\beta \quad \text{on } S_f, \tag{12}$$

$$\frac{ds\varphi}{dt} = \frac{1}{2}\left(\varphi_\alpha^2 + \varphi_\beta^2\right) - \frac{s\beta}{F_r^2} \quad \text{on } S_f, \tag{13}$$

$$\frac{\delta s\varphi}{\delta t} = -\frac{1}{2}\left(\varphi_\alpha^2 + \varphi_\beta^2\right) - \frac{s\beta}{F_r^2} + u\varphi_\alpha - v\varphi_\beta. \tag{14}$$

The far-field boundary condition retains the same form as that in Eq. (9).

C. The pressure and force coefficients

When the boundary integral equation is solved for the potential at each given time step, the pressure p can then be obtained through the Bernoulli equation. In the dimensionless form, the pressure can be written as follows:

$$C_p = \frac{p}{\frac{1}{2}\rho v_0^2(1+\varepsilon^2)} = -\frac{2}{(1+\varepsilon^2)}\left(\phi_t + \frac{1}{2}|\nabla\phi|^2 + \frac{z_0}{F_n^2}\right), \tag{15}$$

where ϕ_t is taken for fixed x_0 and y_0. We note that in the equation, even when the velocity potential φ or ϕ has been obtained at each

time step numerically, ϕ_t is still not explicitly known if the solution is not self-similar. Here, we employ the approach developed by Wu and Eatock Taylor.[26,27] ϕ_t satisfies the Laplace equation. Its free surface boundary condition can be obtained from pressure $p = 0$. The body surface boundary condition for ϕ_t can be written as follows:[28]

$$\frac{\partial \phi_t}{\partial n} = \dot{u} n_{x_0} - \dot{v} n_{y_0} - u \frac{\partial \phi_{x_0}}{\partial n} + v \frac{\partial \phi_{y_0}}{\partial n}. \tag{16}$$

In the stretched system, it takes the form of

$$\frac{\partial \phi_t}{\partial n} = s\dot{u} n_\alpha - s\dot{v} n_\beta - u \frac{\partial \varphi_\alpha}{\partial n} + v \frac{\partial \varphi_\beta}{\partial n}. \tag{17}$$

The normal n in Eqs. (18) and (19) is, respectively, taken from physical system and stretched system. Based on (19), we can define three auxiliary functions

$$\phi_t = \chi_0 + s\dot{u}\chi_1 - s\dot{v}\chi_2 - u\varphi_\alpha + v\varphi_\beta. \tag{18}$$

On the body surface, the auxiliary functions $\chi_i, i = 1, 2, 3$ satisfy the following boundary conditions:

$$\frac{\partial \chi}{\partial n} = 0, \quad \frac{\partial \chi_1}{\partial n} = n_\alpha, \quad \frac{\partial \chi_2}{\partial n} = n_\beta. \tag{19}$$

Using zero pressure condition of free surface, then we have

$$\chi_0 = -\left(\frac{1}{2}|\nabla\varphi|^2 + \frac{s\beta}{F_n^2}\right) + u\varphi_\alpha - v\varphi_\beta, \quad \chi_1 = 0, \chi_2 = 0. \tag{20}$$

At the far field, where the disturbance diminishes, the boundary condition can be written as follows:

$$\frac{\partial \chi}{\partial n} = 0, \quad \frac{\partial \chi_1}{\partial n} = 0, \quad \frac{\partial \chi_2}{\partial n} = 0. \tag{21}$$

The auxiliary functions can then be solved in the stretched co-ordinate system in the same way used for φ. Once they are found, the temporal derivative of ϕ can be obtained from Eq. (18), which can then be used in Eq. (15) for the pressure.

D. The boundary integral equation

We adopt the boundary element method to solve the present problem. The Laplace equation in the fluid domain is first converted into an integral equation over the whole boundary S through Green's identity

$$A(p)\varphi(p) = \int_S \left(\ln r_{pq} \frac{\partial \varphi(q)}{\partial n_q} - \varphi(q) \frac{\partial \ln r_{pq}}{\partial n_q}\right) ds, \tag{22}$$

where $A(p)$ is the solid angle at the point p on the boundary and r_{pq} is the distance from the field point p to the source point q. The integration in (22) is performed with respect to q. The boundary S contains the plate surface S_b, and free surface S_f and a control surface away for the body, where the disturbance to the fluid by the plate is assumed to be insignificant. Linear straight elements are used on the boundary, and the numerical solution of (22) can refer to that in Sun and Wu.[21]

III. NUMERICAL RESULTS AND DISCUSSION

Figure 2 gives a profile of a two-term camber, the deadrise angle γ between the chord and x_0 axis, the frame $O - x_B y_B$, and

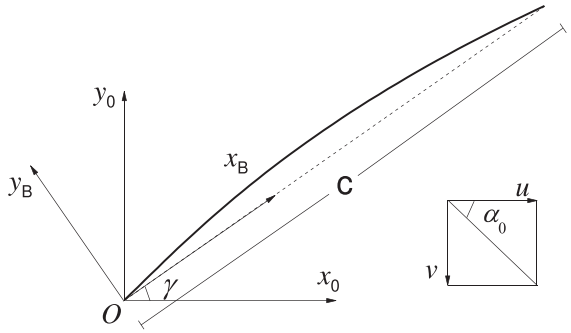

FIG. 2. Two-term camber.[6]

$O - x_0 y_0$ are all defined in Fig. 1. Previous research predominantly concentrated on foils characterized by straight-line or circular arc profiles. However, in practical applications, ventilating propellers often employ a distinct foil profile shape. Among the commonly employed blade profiles for this category of propellers are the two-term camber.[6]

$$y_B = \frac{1}{2}A\left(x_B + \frac{8}{3}x_B^{\frac{3}{2}} - 4x_B^2\right) + Bx_B, \tag{23}$$

in which $0 \le x_B \le c$, in present work, after nondimensionalization, c is taken as 1, A and B parameters are controlling the shape of foil, and we take $A = 0.145\,14$ and $B = 0.024\,19$, which is given in the work by Furuya.[6] Lift coefficient C_p is defined as the force coefficients perpendicular to the motion direction, while drag coefficient is defined as that parallel to the motion direction.

$$C_l = -\sin(\alpha_0)\int_0^{\bar{c}} C_p n_{x_0} dl - \cos(\alpha_0)\int_0^{\bar{c}} C_p n_{y_0} dl, \tag{24}$$

$$C_d = -\cos(\alpha_0)\int_0^{\bar{c}} C_p n_{x_0} dl + \sin(\alpha_0)\int_0^{\bar{c}} C_p n_{y_0} dl. \tag{25}$$

It should be noticed that the integration is along the curved foil surface, and the length of foil profile $\bar{c}$ is larger than the chord length c. To investigate the problem more conveniently, we define another important parameter, which is the attack angle α_A between the direction of incoming flow and foil surface and can be obtained through $\alpha_A = \pi - \alpha_0 - \gamma$. Assuming the foil undertakes a motion with $v = 1 + at$, the foil has an initial vertical entry velocity 1 after nondimensionalization, and setting $u = \varepsilon v = v/\tan\alpha_0$.

A. Convergence study

To test the numerical stability and accuracy of the method in the paper, the case of a foil entering into water vertically is first considered. The stretched system based on the stretched ratio s is used at the initial stage, when s reaches $0.5c$, and the stretched ratio will not change and is kept at $0.5c$, and during this stage, it is equivalent to that the computation is conducted in the physical domain by using length scale $0.5c$ for nondimensionalization. The simulation starts at $s = s_0$. In the work by Sun and Wu[14] for an inclined flat plate entering into water, they concluded that when $\frac{s}{s_0} \ge 20$, the singularity at $t = 0$ will diminish

and will not affect solution after $\frac{s}{s_0} = 20$. This means if s_0 is sufficiently small, the inaccuracy of solution near $t = 0$ will not affect overall results. In present work, we choose $s_0 = 10^{-5}$. The length and the depth of the rectangular computational domain are, respectively, set as 160 and 80 in the stretched system. The ratio of horizontal velocity to vertical velocity $\varepsilon = -0.1$, deadrise angle $\gamma = 45°$, and acceleration a is set as zero. Unequal elements are distributed along the fluid boundary. The body surface and part of the free surface between the jet tip and the plate edge are distributed with elements with equal size, denoted as l_m, and the size of the element along the free surface away from the jet tip and plate increases gradually at a fixed ratio δ and is not allowed to be larger than 5. We set the time increment as $ds = \min[\tau^{n-1} ds_0, l_m/(k|\nabla\varphi|_{\max})]$, where $\tau > 1$ and $k > 1$ are fixed constants, n means the nth time step, and $|\nabla\varphi|_{\max}$ is the largest velocity of fluid particle on the free surface. The first step ds_0 at $n = 1$ is the smallest, and the step then increases at a fixed ratio τ. The step is not allowed to be larger than $l_m/(k|\nabla\varphi|_{\max})$, or a fluid particle is not allowed to move more than a fraction of the element length. Figure 3 gives snapshots of free surface and pressure at $s = 1$ and the histories of lift coefficient and drag coefficient vs vertically traveled distance s, respectively, at $l_m = 0.03$, 0.04, and 0.05; l in the figure is the length along the plate measured from the leading edge A in the physical system, or $l = \sqrt{(x_0 - x_{0A})^2 + (y_0 - y_{0A})^2}$. Curves between different meshes are nearly duplicated, and this verifies that the present procedure is mesh independent.

Figure 4 gives comparison between results at $s = 1$ and the histories of lift and drag coefficients for $\gamma = 45°$, $\varepsilon = -0.1$, and $a = 0$, with two different time steps, setting $l_m = 0.03$ and $\delta = 1.02$. In case 1, $ds_0 = 2.5 \times 10^{-9}$, $k_1 = 20$, and $\tau = 1.001$, and in case 2, $ds_0 = 2.5 \times 10^{-9}$, $k_1 = 40$, and $\tau = 1.0005$. It can be seen that the two curves of free surfaces are graphically indistinguishable, and those of pressure coefficients also coincide well. Both lift coefficients and drag coefficients between two different time steps are in good agreement. This shows the time step convergence of the numerical procedure. Unless it is specified, $ds_0 = 2.5 \times 10^{-9}$, $k_1 = 20$, and $\tau = 1.001$ are used in the following simulations.

B. Comparison

We have not found the direct results for the water entry of two-term camber into water with infinite depth, and the present procedure can both be applied to curved foil and flat foil; thus, we make a comparison with solution of water entry of a flat plate into water with infinite depth by Wang.[5] The work by Wang[5] is for the cases with attack

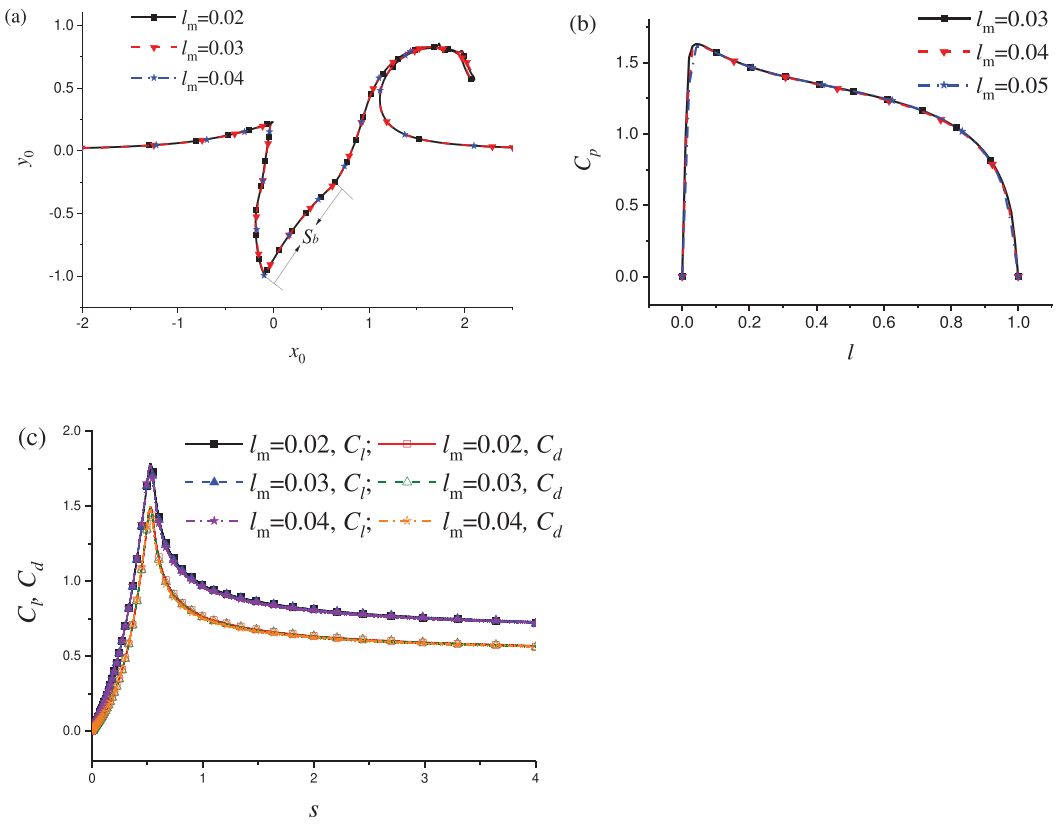

FIG. 3. Mesh convergence study ($\gamma = 45°$, $\varepsilon = -0.1$, and $a = 0$): (a) the free surface profile ($s = 1$), (b) the pressure distribution ($s = 1$) and the histories of lift and drag coefficients vs vertically traveled distance s ($\delta = 1.02$, $ds_0 = 2.5 \times 10^{-9}$, $\tau = 1.001$, and $k_1 = 20$).

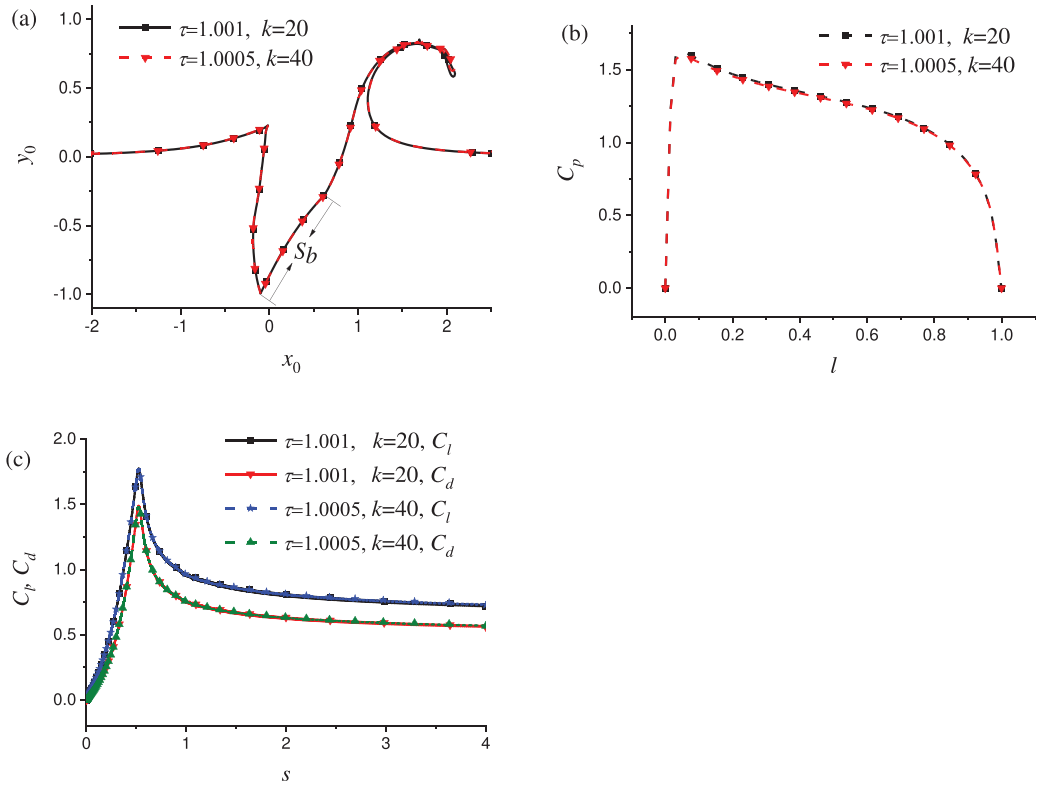

FIG. 4. Time step convergence study ($\gamma = 45°$, $\varepsilon = -0.1$, and $a = 0$): (a) the free surface profile ($s = 1$), (b) the pressure distribution ($s = 1$), and (c) histories of lift and drag coefficients vs vertically traveled distance s ($l_m = 0.03$, $\delta = 1.02$).

angle α_A, and the boundary conditions are all linearized. In present numerical procedure, the deadrise angle γ is set as 35°, $\varepsilon = -1$ ($\alpha_0 = 145°$), $a = 0$, and the corresponding attack angle α_A is 10°. In the work by Wang,[5] they provided the results of $C_f/\alpha_A = \int_0^1 C_p dl/\alpha_A$, and t provided in the figure is nondimensionalized by the chord length c and the resultant velocity $v\sqrt{1+\varepsilon^2}$. Before $t \approx 0.15$, force coefficients rise linearly with entry time t both in present work and Wang,[5] but the former is prominently larger than the latter. In this stage, the fluid obtains momentum from the moving foil in a short time interval, impact pressure due to the large rate of momentum change of fluid takes the dominant role, and the consideration of large deformation of the free surface and the use of stretched system makes the present procedure more precise. As the plate further goes down, the free surface detaches from the upper edge B and the jet root moves beyond B, the rate of momentum change of fluid disturbed by the foil drops, then impact pressure becomes small; thus, there is a drop of force coefficient during $t \approx 0.65$ and 1. After $t \approx 1$, the flow around the plate becomes steady, the force coefficient would not change anymore, and the detailed discussions can also be found in a previous work by Sun and Wu.[14] Before $t \approx 3$, a large difference between two curves can be found, and this is because the use of nonlinear boundary conditions and stretched system would greatly increase the precision of results. After $t \approx 3$, the gap between two results becomes small and the difference becomes stable after $t \approx 6$, and the difference after $t \approx 6$ mainly comes from the difference of boundary conditions. Small gap after $t \approx 3$ further verifies that the present numerical procedure is precise (Fig. 5).

C. Froude number

We now consider the gravity effect through the Froude number defined as $F_n = v/\sqrt{gc}$ for two-term camber and flat foil, as shown in Fig. 6. We undertake simulations at Froude numbers $F_n = 1.597$ and infinity, and in the case of infinite Froude number, gravity is neglected. Let $\gamma = 45°$, $\varepsilon = -0.1(\alpha_0 = 95.67°)$, and the acceleration $a = 0$. In

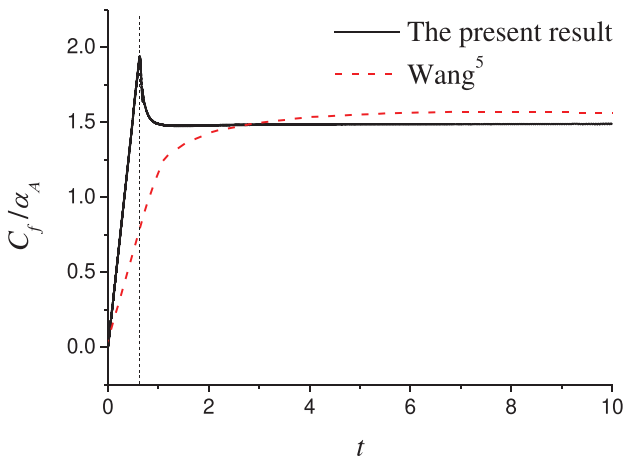

FIG. 5. The time history of force coefficients C_f/α_A ($\varepsilon = -1$, $\gamma = 35°$).

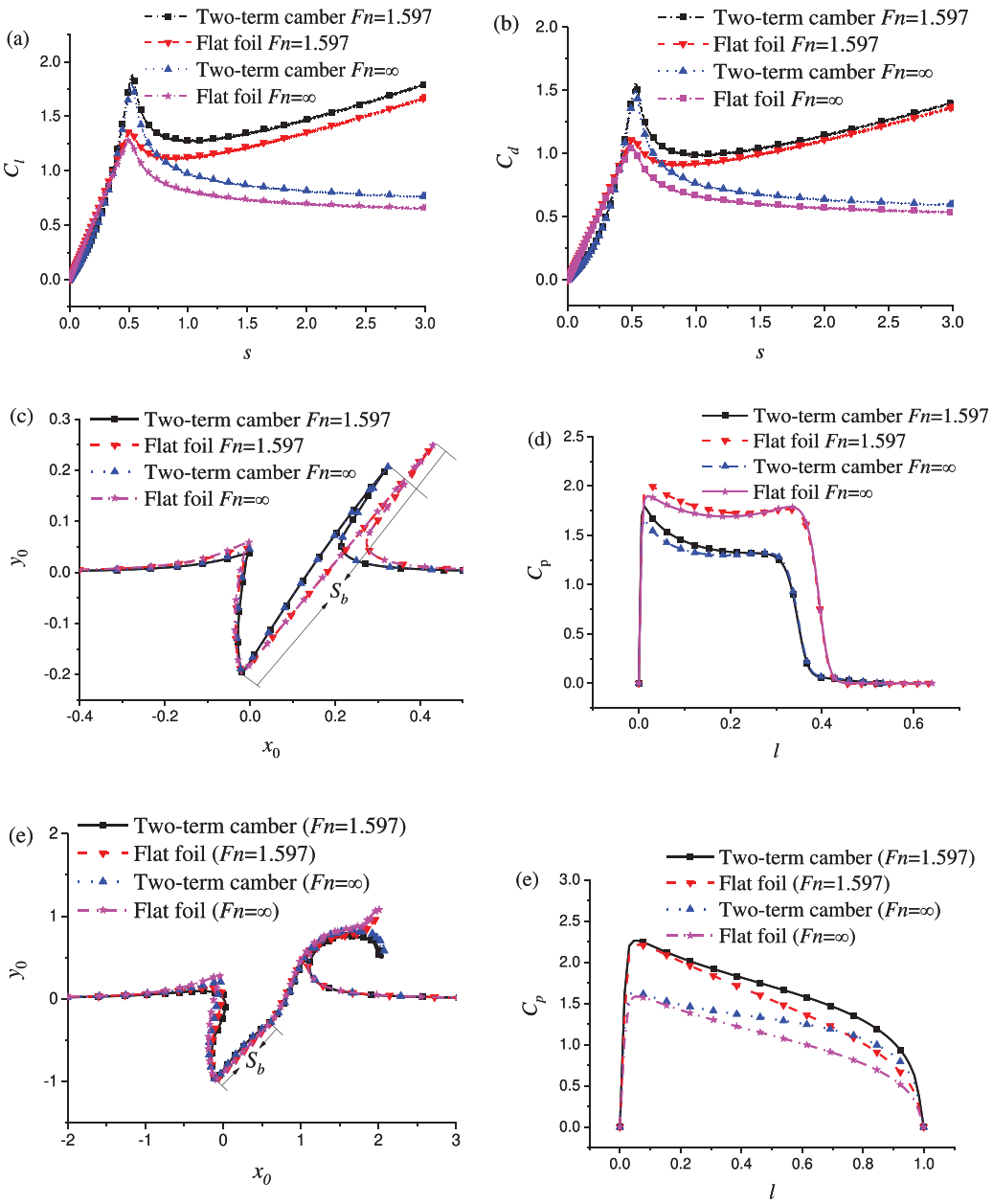

FIG. 6. Water entry of foils with gravity effect ($\gamma = 45°$, $\varepsilon = -0.1$, and $\alpha_0 = 95.68°$): (a) lift coefficient, (b) drag coefficient, (c) free surface ($s = 0.2$), (d) pressure ($s = 0.2$), (e) free surface ($s = 1$), and (f) pressure ($s = 1$).

Figs. 6(a) and 6(b), both lift and drag coefficients increase sharply when s is not large, the coefficients reach a peak at $s \approx 0.6$, and this is because the jet root has reached the trailing edge B, which has been concluded in the work by Sun and Wu.[14] After the jet root exceeds and moves far away from the edge B, impact pressure along the foil would become small, and then, the force coefficients drop quickly. As the foil travels down further, the flow around the foil without gravity gradually becomes steady; thus, the force coefficients with $F_n = \infty$ would not change anymore for larger s, both for curved foil and flat foil. However, the results are quite different for the cases with gravity ($F_n = 1.597$), at which the force coefficients rise linearly with entry distance s, and this is mainly due to the effect of the gravity term in Eq. (15). It can be found that when s is small, the differences of force coefficients between two Froude numbers are also small due to smaller gravity effect. As s increases, the difference becomes increasingly prominent. It can be concluded that the impact effect is important at early stage while the gravity effect is more prominent at later stage, both for curved foil and flat foil.

In Figs. 6(a) and 6(b), it is of great interest to see that during the early stage before $s \approx 0.6$, the force coefficients of flat foil rise linearly with s. While force coefficients of curved foil are smaller than those of flat foil, they rise mildly at first; then, the rise rate becomes increasingly larger, and finally, the force coefficients of curved foil exceed those of flat foil. The intersection point between flat foil and curved foil occurs at $s \approx 0.4$. This is due to the effect of effective deadrise angle; for the two-term camber, the effective deadrise at each point of curved body is quite different. At $s = 0.2$, as seen in Figs. 6(c) and 6(d), the effective deadrise γ of the two-term camber between foil surface and $+x$ axis is larger than that of flat foil, and thus, the pressure of the former is noticeably smaller. This coincides with the conclusion of the work by Sun *et al.*[29] that larger deadrise would result in smaller pressure. As the free surface rises up along the body, the jet root is close to the top edge B or beyond that point, the effective deadrise angle near the edge B is most important in deciding the pressure. Because the point B of two-term camber bends down, the effective deadrise angle at point

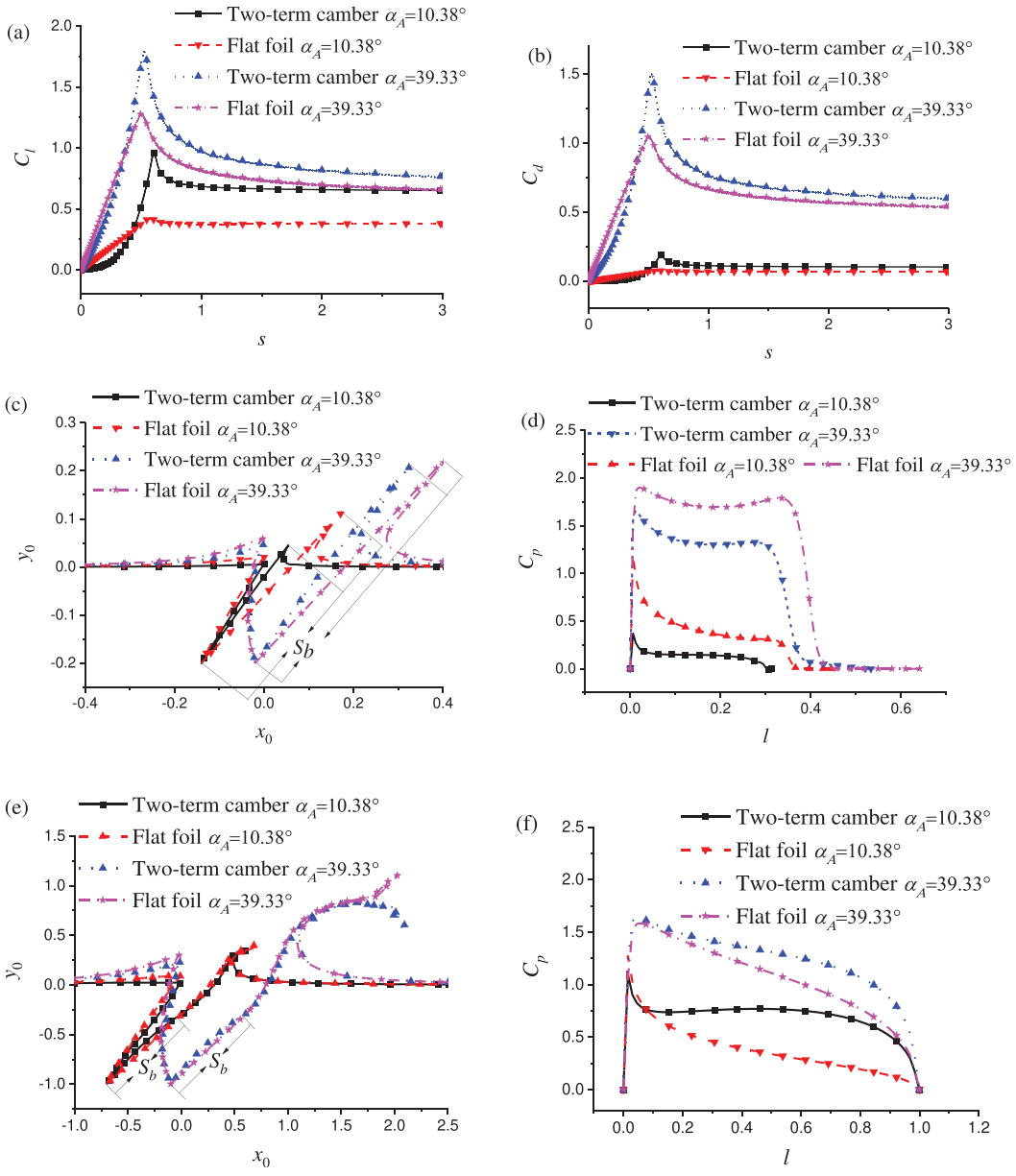

FIG. 7. Water entry of foils with different attack angles ($\gamma = 45°$, $F_n = \infty$): (a) lift coefficient, (b) drag coefficient, (c) free surface ($s = 0.2$), (d) pressure ($s = 0.2$), (e) free surface ($s = 1$), and (f) pressure ($s = 1$).

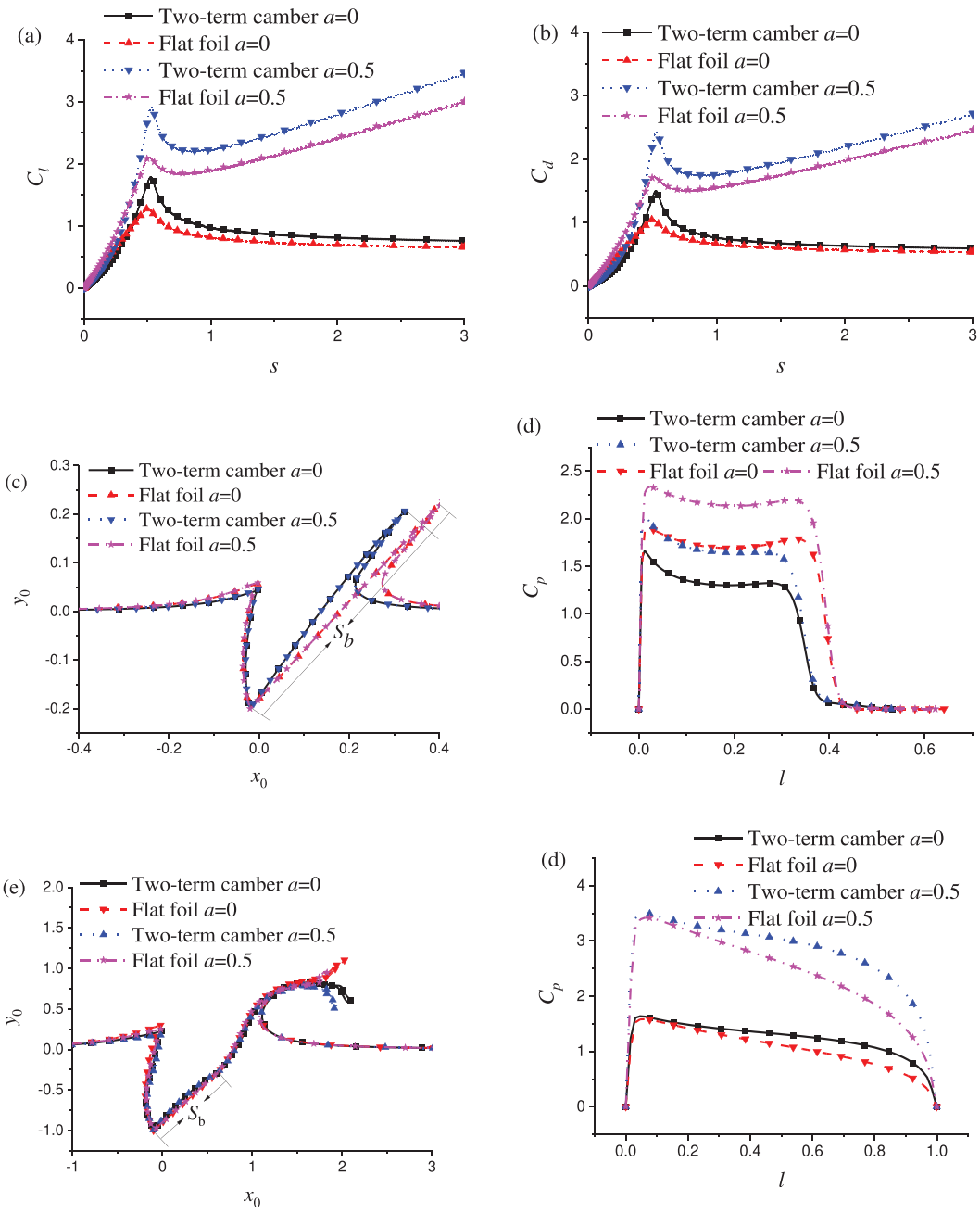

FIG. 8. Water entry of foils with different accelerations ($\gamma = 45°$, $\varepsilon = -0.1$, and $F_n = \infty$): (a) lift coefficient, (b) drag coefficient, (c) free surface ($s = 0.2$), (d) pressure ($s = 0.2$), (e) free surface ($s = 1$), and (f) pressure ($s = 1$).

B then becomes small, and the corresponding pressure therefore becomes large, as seen in Figs. 6(e) and 6(f). In this section, it can be found that curvature of the two-term camber will lead to the variation of the effective deadrise angle γ, the pressure is very sensitive to the deadrise angle or the curvature of the body, and this leads to smaller force coefficients at early stage of water entry and later larger force coefficients.

D. Attack angle

The attack angle α_0 is investigated in this case through setting $\varepsilon = -0.1$ ($\alpha_0 = 95.68°$) and -0.7 ($124.96°$), respectively, the deadrise $\gamma = 45°$, the acceleration $a = 0$, and the corresponding attack angle $\alpha_A = 39.33°$ and $10.38°$, respectively. In Figs. 7(a) and 7(b), force coefficients with smaller attack angle ($\alpha_A = 10.38°$) are noticeably

smaller than those of $\alpha_A = 39.33°$ through the whole process of water entry, and the drop of drag coefficients is more noticeable than that of lift coefficients, and this says the foil with smaller attack angle would show a better performance within the range of attack angle provided in the figure. A milder increase in the force coefficients at first can also be found in all attack angles, the reason for this is due to the variation of effective deadrise angle along the curved body, which has been explained in Sec. III C. However, the difference in force coefficients between curved foil and flat foil for the case with a smaller attack angle seems more prominent. This is because the ratio of the variation of deadrise angle to the attack angle is larger for smaller attack angles, and thus, the pressure is more sensitive to the variation of the effective deadrise angle. This can be found in Fig. 7(c), the angle of the flat foil between the free surface and body is approximately twice that of curved foil at $\alpha = 10.38°$, such a difference originates from the curvature, and the corresponding pressure in Fig. 7(d) of flat foil is about twice that of the two-term camber. In Figs. 7(e) and 7(f), the effective deadrise angle near edge B becomes important, the two-term camber with smaller effective deadrise angle would gain a larger impact pressure, and also for smaller attack angle, the difference of pressure between curved body and flat body is more prominent.

E. Acceleration

The effect of acceleration a is investigated in the present case, the deadrise $\gamma = 45°$, $\varepsilon = -0.1$, and the gravity effect is neglected through setting $F_n = \infty$, and the acceleration a is taken as 0 and 0.5, respectively. In Figs. 8(a) and 8(b), both the lift and drag coefficients with acceleration $a = 0.5$ are noticeably larger than that of $a = 0$. Without gravity, flow around the foil will eventually become stable and the force coefficient will tend to a constant when s is large enough. However, once considering gravity, the force coefficient will rise linearly with entry distance s due to the effect of inertial force. It is of interest to see that the free surfaces in Figs. 8(c) and 8(e) between different accelerations are nearly duplicated, but the pressure between different accelerations in Figs. 8(d) and 8(f) varies much, and this means the pressure is more sensitive to accelerations.

IV. CONCLUSIONS

The problem of a curved foil entering into calm water is investigated through the velocity potential flow theory together with the boundary element method in time domain, and the stretched coordinate system method and auxiliary method are used. The effects of gravity, attack angle, and acceleration are investigated and discussed. From these, the following conclusions can be drawn.

(1) When the foil either with curved shape or flat shape enters water suddenly, the water is suddenly disturbed, the momentum of fluid would change in a short time interval, and then, a larger impact pressure would form along the body. Since the gravity needs time to take effect, in the early stage, the impact effect is more important, while at a later stage, the fluid around the plate gradually becomes stable, the impact pressure drops, and the gravity effect then becomes more prominent.
(2) Curvature of the two-term camber would lead to the variation of the effective deadrise angle γ in water entry, and this would result in a noticeable variation of pressure. At early stage of water entry, the smaller effective deadrise angle at the leading edge A takes a major effect, and the pressure is then smaller. When the jet root is close to or beyond the trailing edge B, the smaller effective deadrise angle would lead to larger pressure.
(3) With the range of attack angle provided in the present paper, the force coefficients with smaller attack angle are also smaller, but since the decrement in the drag coefficient is more prominent, the foil with smaller attack angle would gain a better performance.
(4) For the foil with a smaller attack angle, the pressure is more noticeably affected by the variation of effective deadrise angle.
(5) The considering of acceleration does not have a significant effect on the free surface, but it does have a significant effect on the pressure.

ACKNOWLEDGMENTS

This work is supported by the National Natural Science Foundation of China (Grant No. 52271276).

AUTHOR DECLARATIONS

Conflict of Interest

The authors have no conflicts to disclose.

Author Contributions

Shi Yan Sun: Supervision (equal); Writing – original draft (equal). **Fanrong Zeng:** Data curation (equal). **Yifeng Yang:** Supervision (equal); Writing – review & editing (equal). **Wenli Wang:** Data curation (equal).

DATA AVAILABILITY

The data that support the findings of this study are available within the article.

REFERENCES

[1] J. N. Newman, *Marine Hydrodynamics* (The MIT Press Cambridge, Massachusetts, 2017).
[2] B. Yim, "An application of linearized theory to water entry and water exit problem. Part 2 (with ventilation)," Research and Development Report No. 3171 (Naval Ship Research and Development Center, Washington, DC, 1970).
[3] B. Yim, "Linear theory on water entry and exit problems of a ventilating thin wedge," J. Ship Res. **18**, 1–11 (1974).
[4] D. P. Wang, "Water entry and exit of a fully ventilated foil," J. Ship Res. **21**, 44–68 (1977).
[5] D. P. Wang, "Oblique water entry and exit of a fully ventilated foil," J. Ship Res. **23**, 43–54 (1979).
[6] O. Furuya, "A performance-prediction theory for partially submerged ventilated propellers," J. Fluid Mech. **151**, 311–335 (1985).
[7] Y. L. Young and S. A. Kinnas, "Analysis of supercavitating and surface-piercing propeller flows via BEM," Comput. Mech. **32**, 269–280 (2003).
[8] E. Yari and H. Ghassemi, "Hydrodynamic analysis of the surface-piercing propeller in unsteady open water condition using boundary element method," Int. J. Nav. Archit. Ocean Eng. **8**, 22–37 (2016).
[9] B. S. Chekin, "The entry of a wedge into an incompressible fluid," J. Appl. Math. Mech. **53**, 300–307 (1989).
[10] M. Savineau, "A time marching boundary element method for the prediction of the flow around surface piercing hydrofoils," Master's thesis (Massachusetts Institute of Technology, 1996).
[11] O. M. Faltinsen and Y. Semenov, "Nonlinear problem of flat-plate entry into an incompressible liquid," J. Fluid Mech. **611**, 151–173 (2008).

[12]V. Vinayan and S. Kinnas, "A numerical nonlinear analysis of two-dimensional ventilating entry of surface-piercing hydrofoils with effects of gravity," J. Fluid Mech. **658**, 383–408 (2010).
[13]Y. T. Wu, "A free streamline theory for two-dimensional fully cavitated hydrofoils," J. Math. Phys. **35**, 236–265 (1956).
[14]S. Y. Sun and G. X. Wu, "Oblique water entry of an inclined finite plate with gravity effect," Phys. Fluids **35**, 042112 (2023).
[15]P. Ghadimi and N. Javanmardi, "Analysis of ventilation regimes of the oblique wedge-shaped surface piercing hydrofoil during initial water entry process," Pol. Marit. Res. **25**, 33–43 (2018).
[16]N. Javanmardi and P. Ghadimi, "Hydroelastic analysis of surface piercing hydrofoil during initial water entry phase," Sci. Iran. **26**, 295–310 (2019).
[17]J. D. Mesa, K. J. Maki, and M. T. Graham, "Numerical analysis of the impact of an inclined plate with water at high horizontal velocity," J. Fluids Struct. **114**, 103684 (2022).
[18]A. Iafrati and A. A. Korobkin, "Initial stage of flat plate impact onto liquid free surface," Phys. Fluids **16**, 2214 (2004).
[19]A. Iafrati and A. A. Korobkin, "Hydrodynamic loads during early stage of flat plate impact onto water surface," Phys. Fluids **20**, 082104 (2008).
[20]R. Krechetnikov, "Origin of ejecta in the water impact problem," Phys. Fluids **26**, 052105 (2014).
[21]S. Y. Sun and G. X. Wu, "Local flow at plate edge during water entry," Phys. Fluids **32**, 072103 (2020).
[22]C. N. Cui, R. Han, S. C. Pei, and S. P. Wang, "Jet characteristics of the three-dimensional explosion bubble in a compressible fluid," Phys. Fluids **35**, 082123 (2023).
[23]S. P. Wang, A. M. Zhang, Y. L. Liu, S. Zhang, and P. Cui, "Bubble dynamics and its applications," J. Hydrodyn. **30**, 975–991 (2018).
[24]S. P. Wang, A. M. Zhang, Y. L. Liu, and D. R. Zeng, "Numerical simulation of bubble dynamics in an elastic vessel," Eur. Phys. J. E **36**, 119 (2013).
[25]G. X. Wu, H. Sun, and Y. S. He, "Numerical simulation and experimental study of water entry of a wedge in free fall motion," J. Fluids Struct. **19**, 277–289 (2004).
[26]G. X. Wu and R. Eatock Taylor, "Transient motion of a floating body in steep waves," in Proceedings of 11th Workshop on Water Waves and Floating Bodies, Hamburg, Germany (1996).
[27]G. X. Wu, "Hydrodynamic force on a rigid body during impact with liquid," J. Fluids Struct. **12**, 549–559 (1998).
[28]G. X. Wu and R. Eatock Taylor, "The coupled finite element and boundary element analysis of nonlinear interactions between waves and bodies," Ocean Eng. **30**, 387–400 (2003).
[29]S. Y. Sun, S. L. Sun, and G. X. Wu, "Oblique water entry of a wedge into waves with gravity effect," J. Fluids Struct. **52**, 49–64 (2015).